

Optimization of charging process for electric micromobility devices with real-time operation

Jiacheng He ^{*} , Theodoros Kalogiannis, Xia Zeng , Md Sazzad Hosen , Maitane Bercibar

ETEC Departement & MOBI Research Group, Vrije Universiteit Brussel (VUB), Pleinlaan 2, 1050 Brussel, Belgium

ARTICLE INFO

Keywords:

Fast charging
E-micromobility devices
Lithium-ion batteries
Thermal management system
Dynamic programming

ABSTRACTS

While fast charging offers undeniable benefits in user convenience, it also presents significant challenges, particularly concerning the thermal management of batteries. The e-micromobility devices, such as e-bikes and e-motorcycle, often use cost-efficiency processors and passive cooling due to cost considerations, which makes it difficult for existing optimization algorithms to run reliably on these devices. To tackle these challenges, this study proposed an optimized charging algorithm for those devices. To meet the need for low computational efforts in real-N

time usage, the proposed algorithm incorporates both offline training and online operation. During offline training, by considering a trade-off between charging time and temperature variations, optimized charging current policy maps are obtained based on the 1D electrothermal model and dynamic programming. When operation online, the processor only needs to interpolate the optimized policy charging map. The obtained optimized policy maps are further validated in real-time experiments with a 43Ah battery. The experiment results show that, compared to the benchmark 1C constant current charging, the charging time is reduced by 8.5 % with the proposed charging strategies, while the charged State of Charge (SoC) and temperature increases remain nearly identical. Robust analysis demonstrates that the algorithm remains stable and effective under different room-temperature and SoC conditions. Moreover, for real-time operation, a minimum execution time of 0.44 milliseconds on an 8-bit microcontroller demonstrates the method's suitability for low-cost e-micromobility application.

1. Introduction

Lithium-ion batteries (LIBs) are widely utilized in electric transportation because of their high energy density and long cycle life [1]. However, as the current demand increases, the energy density of LIBs also rises, leading to significant heat generation when the batteries operate under various conditions [2]. Hence, ensuring the safety of LIBs operating at high currents has become a critical concern due to the potential risk of thermal runaway [2–4]. To keep battery temperature within the safety range during fast charging, many studies have explored the optimization of battery thermal management systems to enhance heat dissipation [5,6]. Beyond thermal management, numerous scholars have conducted in-depth research on battery charging strategies [7,8].

Generally, charging strategies can be classified into closed-loop and open-loop optimization [7,8]. In the open-loop approach, a predefined current profile is applied regardless of the battery condition, which makes the strategy simple and hardware-efficient but less adaptable.

Conversely, closed-loop approaches adjust the charging profile according to the real-time battery state, thereby improving safety and prolonging lifetime, despite the increased computational complexity [7,8]. In the context of closed-loop strategies, Duan et al. [9] introduced a PID-based closed-loop constant-temperature control integrated with a multi-objective biogeography-based optimization algorithm, demonstrating that the charging process can be accelerated without additional states of health (SOH) degradation compared to the traditional CC–CV protocol. Similarly, Shen et al. [10] developed a coupled Simulink–Fluent framework that considers both temperature rise and lithium plating boundaries, achieving a 48 % reduction in charging time while maintaining the maximum temperature below 50 °C. Extending these efforts, Sayed et al. [11] employed reinforcement learning to dynamically adapt charging currents according to real-time battery states, thereby balancing charging speed with temperature control and health preservation. In a similar direction, Hind et al. [12] proposed a deep reinforcement learning framework for multi-stage constant current

^{*} Corresponding author.

E-mail address: Jiacheng.He@vub.be (J. He).

<https://doi.org/10.1016/j.rineng.2025.107826>

Received 16 June 2025; Received in revised form 3 October 2025; Accepted 18 October 2025

Available online 18 October 2025

2590-1230/© 2025 The Authors. Published by Elsevier B.V. This is an open access article under the CC BY license (<http://creativecommons.org/licenses/by/4.0/>).

charging, which learns optimal current profiles under electro-thermal constraints and demonstrates robust performance across varying electrode configurations. Building on these advances, Chen et al. [13] introduced a safety-aware deep reinforcement learning approach based on distributional soft actor-critic with conservative augmented Lagrangian, explicitly embedding thermal and health constraints to enhance robustness, ensure safe operation, and mitigate long-term capacity degradation compared to conventional strategies.

Although closed-loop approaches provide high adaptability and are commonly applied in electric vehicles with advanced processors, their considerable computational requirements constrain their use in cost-sensitive systems typically governed by cost-effective microcontrollers [14–16]. However, for e-mobility devices such as scooters or e-bikes, cost-effective microcontrollers are typically used due to cost limitations. Therefore, the application of closed-loop approaches in such devices is limited, and open-loop strategies are generally adopted due to their lower computational requirements and simpler implementation.

Among them, the Multi-Stage Constant Current (MSCC) method is widely used, in which the charging process is divided into several constant-current stages with predefined C-rates (C). By progressively reducing the charging current across stages, MSCC can shorten charging time while alleviating polarization and heat accumulation. For example, Lee et al. [17] employed a Taguchi–PSO approach to design a four-stage profile that reduced charging time from 119 min (CC–CV) to 67 min while maintaining comparable efficiency. Building on this, Jiang et al. [18] extended the Taguchi method to five stages, showing 2–3 % higher efficiency and a notable reduction in peak temperature relative to both CC–CV and earlier stage patterns. Wu et al. [19] further demonstrated that a five-stage scheme charged a 20 Ah LFP cell from 20 % to 100 % State of Charge (SOC) in 30 min with controlled temperature rise and negligible lifetime penalty. Kumar and Pareek [20] integrated Grey relational analysis to identify a five-stage pattern that shortened charging time from 73.5 min (Constant Current – Constant Voltage (CC–CV), 0.05 C cut-off) to 48.1 min while also lowering heat generation. More recently, Huang et al. [21] optimized SOC-based transitions with a coyote algorithm, reducing the charging time from 83.6 min (CC–CV) to 55.2 min and substantially lowering the temperature rise. Tahir et al. [22] advanced this line by introducing unequal SOC intervals, achieving faster charging while maintaining thermal behavior comparable to CC–CV.

Despite the improved performance of open-loop strategies like MSCC, their inability to adapt to real-time battery conditions remains a key limitation. In contrast, closed-loop methods allow dynamic adjustment based on the actual battery state, offering improved safety and efficiency. However, such approaches typically require significant computational resources, making them less suitable for cost-effective microcontrollers commonly used in electric scooters and e-bikes.

To address this challenge, this study proposes a hybrid optimization framework that combines offline modeling with lightweight online inference. This approach enables adaptive current control during fast charging without requiring intensive real-time computation. During the offline training, an electro-thermal model is developed considering both reversible and irreversible heat generation during battery charging. The charging process is discretized into N intervals based on the SoC, and for each interval, a range of initial conditions, defined by SoC, temperature and current, were simulated. Using the developed model, the thermal responses under various initial conditions were calculated, forming a comprehensive grid of state transitions. A cost function is then applied to each state-action pair to evaluate the trade-off between temperature rise and charging time. Based on the cost map, dynamic programming is used to derive the optimal charging current at each state, leading to a policy map that minimizes both thermal stress and total charging duration. In real-time running, the processor only needs to interpolate the trained policy map based on the current state of the battery to obtain the optimized charging current. It has been verified that the proposed algorithm exhibits good robustness, efficiently charging the battery to

the desired SoC under different room-temperature and SoC conditions.

In summary, the main contributions of this paper are summarized as follows: 1. A lightweight fast-charging optimization framework is proposed for micromobility devices, designed to run efficiently on cost-effective microcontrollers commonly used in e-scooters and e-bikes. 2. An offline–online strategy is introduced, where a dynamic programming-based policy map enables real-time current control with minimal computational effort. 3. Experimental and implementation results demonstrate good robustness under varying SoC and room-temperature conditions, with a minimum execution time at the sub-millisecond level confirmed on both 8-bit and 32-bit processors. The remainder of this paper is organized as follows: Section 2 describes the system and model development. Section 3 presents the development and implementation of the optimized charging algorithm. Section 4 introduces the experimental setup. Section 5 discusses the experimental results together with the robustness analysis. Finally, Section 6 concludes the paper.

2. System and model development

The goal of this study is to optimize the charging strategy for electric micromobility devices, such as e-bikes and e-scooters, which typically use passive cooling systems. The battery heat distribution path in these devices is shown in Fig. 1. The heat generated by irreversible and reversible heat first causes the battery temperature to rise, and then some of the heat is dissipated into the environment by natural convection when the battery temperature is higher than the ambient temperature.

2.1. Battery thermal model

The transient thermal behavior of lithium-ion batteries has been investigated using both lumped and CFD models. And studies have shown that reversible heat contributes non-negligibly during fast charging [23,24]. To improve dynamic accuracy for thermal optimization, this study incorporates both irreversible and reversible heat into the lumped thermal model, expressed as:

$$m_{bat} C_{pbat} \frac{dT_{bat}}{dt} = \dot{Q}_{ire} + \dot{Q}_{rev} - \dot{Q}_{amb} \quad (1)$$

where m_{bat} is the battery mass (kg), C_{pbat} is the specific heat capacity of the battery (J/kg), T_{bat} is the battery temperature (°C), \dot{Q}_{ire} is irreversible heat rate (W), \dot{Q}_{rev} is the battery reversible heat rate (W) and \dot{Q}_{amb} is heat rate transferred to the ambient (W). Typically, irreversible heat is associated with the battery's ohmic heat loss and is calculated based on the battery open circuit voltage (V_{OCV}), battery terminal voltage (V_{bat}) and current (I_{bat}), as presented below:

$$\dot{Q}_{ire} = |I_{bat}(V_{OCV} - V_{bat})| \quad (2)$$

The reversible heat in the battery arises from the electrochemical reaction and is determined by the current, battery temperature and the derivative of battery open circuit voltage with respect to temperature.

$$\dot{Q}_{rev} = I_{bat} T_{bat} \frac{\partial V_{OCV}}{\partial T_{bat}} \quad (3)$$

The heat rate transferred to the ambient is calculated based on the Newton's law of cooling.

$$\dot{Q}_{amb} = hA(T_{bat} - T_{amb}) \quad (4)$$

where h is the convective coefficient, A is the surface area of the battery and T_{amb} is the ambient temperature. By taking Eqs. (2), (3) and (4) into (1) the thermal model of the battery is shown as below:

$$m_{bat} C_{pbat} \frac{dT_{bat}}{dt} = |I_{bat}(V_{OCV} - V_{bat})| + I_{bat} T_{bat} \frac{\partial V_{OCV}}{\partial T} - hA(T_{bat} - T_{amb}) \quad (5)$$

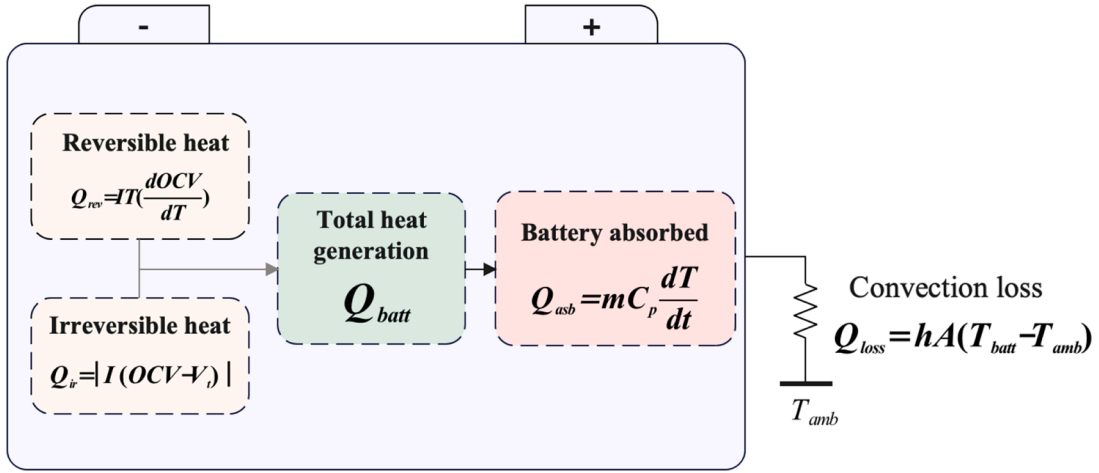


Fig. 1. Schematic of the battery under natural convection.

In this equation, to establish the relationship between the open circuit voltage (OCV) and temperature, the battery is positioned in a climate chamber and measured under various ambient temperatures. The battery current and terminal voltage are obtained from the electrical model described in the following section, while the convective coefficient h is determined based on our previous studies [25,26].

2.2. Battery electric model

The equivalent circuit model (ECM), based on Thevenin's theorem, offers a cost-effective approach for battery voltage estimation. To balance accuracy and computational efficiency, this study adopts a single RC pair, which is sufficient under low-dynamic or constant current profiles [27,28]. As shown in Fig. 2, the terminal voltage (V_{bat}) is derived from Kirchhoff's laws: [27]

$$V_{bat} = V_{ocv} - I_{bat}R_0 - V_{R1} \quad (6)$$

where R_0 is the Ohmic resistance, V_{R1} is the voltage of the RC pair. In this question, both open-circuit voltage (V_{ocv}) and R_0 considered as a nonlinear function of SoC and temperature. The V_{R1} are represented by the following equation:

$$\frac{dV_{R1}}{dt} = \frac{I_{bat}}{C_1} - \frac{V_{R1}}{R_1 C_1} \quad (7)$$

where R_1 and C_1 is the resistor and capacitor in the RC pairs. The value of R_1 , C_1 and OCV varies with the battery SoC, and the SoC is calculated by coulomb counting as:

$$\frac{dSoC}{dt} = -\frac{\eta_c \cdot I_{bat}}{3600 C_{bat}} \quad (8)$$

where η_c is the coulomb efficiency, C_{bat} is the actual capacity in Ah. Generally, to determine values of OCV, R_0 , R_1 and C_1 , hybrid pulse power characterization (HPPC) and OCV-SoC tests are conducted at

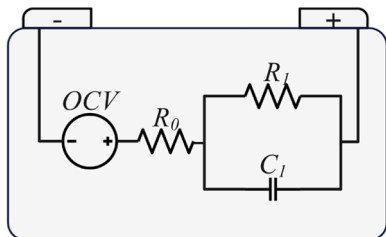


Fig. 2. Equivalent circuit model with one RC.

different SoCs and temperatures. And a table can be formed based on SoC and temperature to save the values determined through HPPC.

2.3. Electric thermal coupling

The coupled model between the electrical and thermal models is shown in Fig.3. Parameters required for the ECM are interpolated from tables based on temperature and SoC. These parameters are usually determined by the HPPC and stored in the form of lookup tables [26]. The ECM calculates the battery terminal voltage from the total current and interpolated values of R_0 , R_1 and C_1 and OCV. The calculated value of terminal voltage, along with the OCV and current, is passed to the thermal model. After receiving input values from the electrical model, the thermal model calculates the battery temperature using the previously presented equations. The calculated temperature value is then sent back to the electrical model as an input for the next iteration.

3. Fast charging temperature trajectory optimization

3.1. Problem formulation

The goal of this paper is to optimize the charging strategy under natural convection for electromobility systems lacking advanced cooling systems. Normally, the battery heat generation rate is not only related to the ambient temperature but also to the battery SoC. This means the battery will have different heat generations under different ambient conditions and states. This means it is possible to increase the charging current in the low heat generation period and decrease the charging current in the high heat generation period, thus reducing the charging time while maintaining the same temperature rise. Hence, the optimization problem is described as dividing the battery charging state into N steps based on the battery SoC and adapting the charging current at each step to optimize the charging time and the battery temperature rise, as indicated by the following equation.

$$\mathcal{J} = \min \left[\sum_{k=1}^N [\alpha_1 L_{Tcost,k}(T_{bat}) + \alpha_2 L_{tcost,k}(T_{bat})] \right] \quad (9)$$

where the $L_{Tcost,k}$ denotes the temperature increase at k^{th} step, $L_{tcost,k}$ denotes the elapsed time from k^{th} to $(k+1)^{th}$ step, α_1 and α_2 are the weighting factors for temperature increases and time used, respectively.

3.2. Dynamic programming optimization strategy design

DP is a mathematical optimization method based on Bellman's principle which aims to reconstruct complex decision problems into a

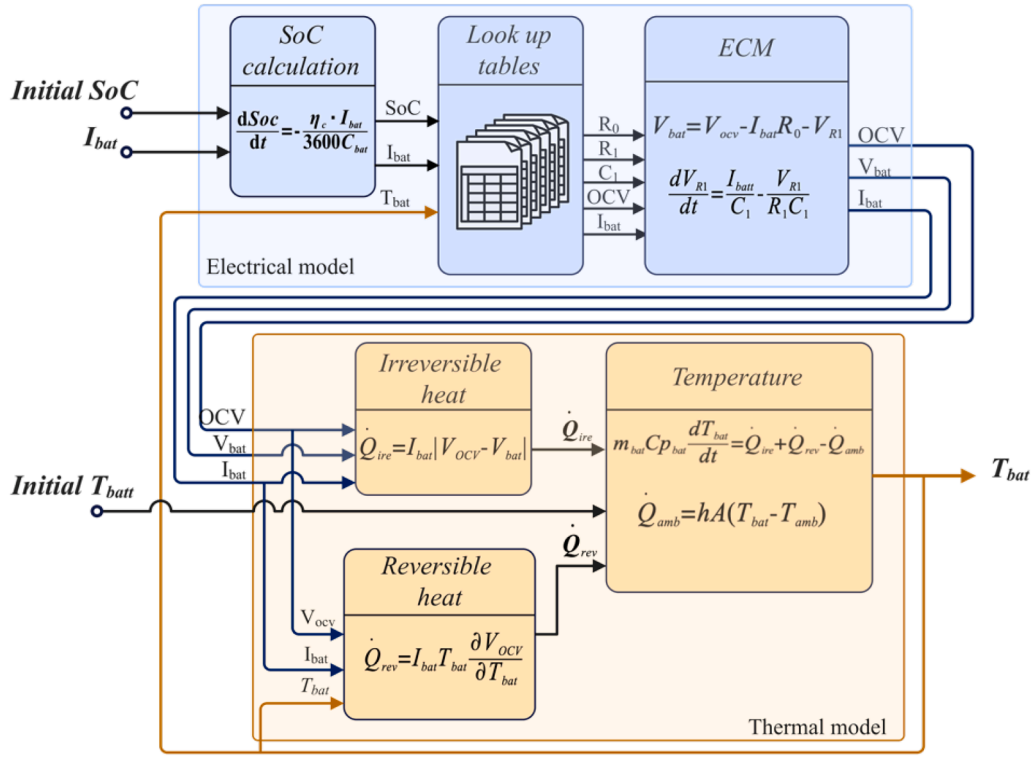


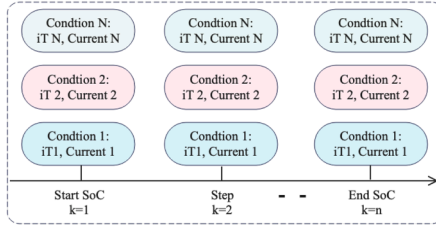
Fig. 3. Coupled electrical and thermal models.

series of more manageable sub-stage decision problems. The optimal solution to this complex problem is then obtained by combining the optimal solution to each sub-problem. Due to the complexity of the model, it could require a large computational effort, making it difficult to use online optimization. However, the optimal solution can be obtained by offline optimization and storing the optimization results in a

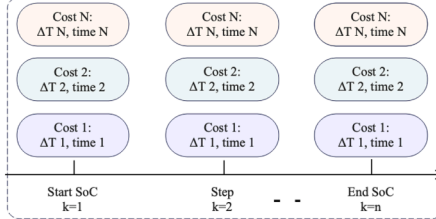
policy map. When running in real-time, the charging current are obtained by looking up the policy map based on the battery status shown in Fig.4.

As presented in Eq. (9), the charging process is initially segmented into N steps with a charging specific SoC range. Each step is denoted by k , where $k = 1, 2, \dots, N$. To minimize temperature rise and charging

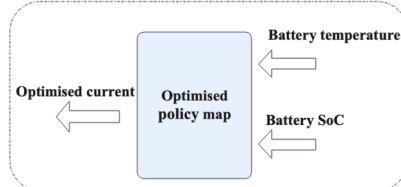
a. Initial state grid



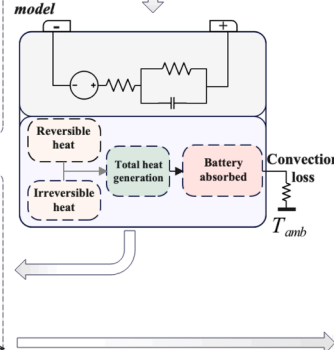
c. Cost grid



f. Online(real-time) running



b. Developed model



e. Optimized policy map

T - SoC	10	20	...	70	80
25	55	55	...	55	55
26	55	55	...	55	55
27	55	55	...	49.5	55
...
38	27.5	27.5	...	22	16.5
39	22	27.5	...	22	11
40	22	22	...	16.5	11

d. Optimisation algorithm

Algorithm 1 Dynamic programming optimizer

Input: $stateSpace_T$ battery state space temperature based on different initial temperature, current and SoC; $stateSpace_t$ space of used charging time based on different initial temperature, current and SoC; $iVecT$ vector of battery initial temperature; $iVecC$ vector of battery charging current; $iVecS$ vector of battery SoC; nK total SoC steps.

Output: $costMap$, $trackMap$ optimized cost map and charging current map from the current SoC to the final SoC.

```

1:  $nS \leftarrow \text{length of SoC temperature vector}$ 
2:  $nT \leftarrow \text{length of initial temperature vector}$ 
3:  $nC \leftarrow \text{length of current temperature vector}$ 
4:  $k \leftarrow nK$ 
5: initial  $costMap$  with  $\text{Inf}(nT, nS)$ 
6: initial  $trackMap$  with  $\text{Inf}(nT, nS)$ 
7: while  $k \neq 0$  do
8:   for  $j \rightarrow 1$  to  $nT$  do
9:     for  $i \rightarrow 1$  to  $nC$  do
10:      if  $k = nK$  then
11:         $iT \leftarrow iVecT(j)$ 
12:         $std \leftarrow iVecT(j_{ind})$ 
13:         $costMap(j, k) \leftarrow K_f(iT - std)$ 
14:         $trackMap(j, k) \leftarrow iVecC(i_{ind})$ 
15:      else
16:         $t \leftarrow stateSpace\_t(i, j, k)$ 
17:         $T \leftarrow stateSpace\_T(i, j, k)$ 
18:         $std\_t \leftarrow stateSpace\_t(i_{ind}, j, k)$ 
19:         $std\_T \leftarrow stateSpace\_T(i_{ind}, j, k)$ 
20:         $deltaT \leftarrow T - iVecT(j)$ 
21:         $std\_deltaT \leftarrow T - iVecT(j_{ind})$ 
22:         $iCost \leftarrow K_i(t - std\_t)$ 
23:         $TCost \leftarrow K_T(T - std\_T)$ 
24:         $cCost \leftarrow iCost + TCost$ 
25:         $pCost \leftarrow \text{interpolate } costMap(:, k+1) \text{ based on } T$ 
26:         $totalCost \leftarrow cCost + pCost$ 
27:        if  $totalCost \leq costMap(j, k)$  then
28:           $costMap(j, k) \leftarrow totalCost$ 
29:           $trackMap(j, k) \leftarrow iVecC(i)$ 
30:        end if
31:      end if
32:    end for
33:  end for
34:  $k \leftarrow k-1$ 
35: end while

```

Fig. 4. Overview of the optimization procedure.

time, the optimization problem is further formulated as follows:

$$J^k = \min_{I_{bat}} [Q^k(I_{bat}, T_{bat}) + J^{k+1}(T'_{bat})], \quad k \in [1, N-1] \quad (10a)$$

$$J^k = K_f(T_{bat} - T_{bat}^*), \quad k = N \quad (10b)$$

where J^k is the minimize at k^{th} step, Q^k is the cost map at k^{th} step, I_{bat} is the charging current at k^{th} step, T_{bat} is the battery initial temperature, T'_{bat} is the battery temperature after this charging step, T_{bat}^* is the battery temperature under a standard constant current charging condition at the end of charging. The step cost Q^k at the k^{th} step is the sum of the time cost Q_t^k with weight factor K_t and the temperature rise cost Q_T^k with weight factor K_T .

$$Q^k = K_T Q_T^k(I_{bat}, T_{bat}) + K_t Q_t^k(I_{bat}, T_{bat}), \quad k \in [1, N-1] \quad (11)$$

The step costs of Q_T^k and Q_t^k are obtained based on a standard CC charge:

$$Q_T^k = C_{mT}(I_{bat}, T_{bat}, k) - C_{mT}(I_{bat_Std}, T_{bat}, k), \quad k \in [1, N-1] \quad (12c)$$

$$Q_t^k = C_{mt}(I_{bat}, T_{bat}, k) - C_{mt}(I_{bat_Std}, T_{bat}, k), \quad k \in [1, N-1] \quad (12d)$$

where, C_{mT} represents the battery temperature increase at the k^{th} step, which depends on its specific initial conditions (e.g., current and temperature). Similarly, C_{mt} represents the time used at k^{th} charging step, and I_{bat_Std} is the selected standard constant charge current.

The weight factors K_T and K_t are constrained to sum to unity ($K_T + K_t = 1$). Increasing K_T emphasizes minimizing temperature rise, while increasing K_t prioritizes shortening charging time. Their complementary adjustment enables balancing safety and efficiency in the optimization process. Meanwhile, the cost components of time and temperature are individually normalized between 0 and 1 using the following equation:

$$x_{norm} = \frac{x - x_{min}}{x_{max} - x_{min}} \quad (13)$$

where x denotes the original data, x_{min} and x_{max} are the minimum and maximum values in the dataset, respectively, and x_{norm} is the normalized result scaled between 0 and 1.

3.3. Charging state discretization and policy map

Sensitivity analyses are conducted for the discretization of SoC, temperature, and current. For the SoC interval, reducing the step from 4 % to 1 % gradually improves the optimization outcome by about 3 %, and since a 1 % resolution is standard in e-mobility devices, a 1 % interval is selected. For the temperature discretization, decreasing the step from 4 °C to 2 °C yields an improvement of approximately 2 %, while a further reduction to 1 °C provides only an additional 0.5 %; therefore, a step size of 2 °C is adopted to balance accuracy and computational efficiency. For the current discretization, four intervals (0.45 C, 0.2 C, 0.1 C, and 0.05 C) are tested, where C denotes the nominal charge/discharge rate defined with respect to the rated capacity of the cell, corresponding to a current of $1C = 1 \times \text{capacity (Ah)}$. For example, a 1 C rate fully charges or discharges the battery in one hour. Since no further improvement is observed once the step reaches 0.2 C, a 0.2 C interval is chosen.

Meanwhile, a two-step sweep is employed to determine the parameters K_T and K_t . First, a coarse search with an interval of 0.1 is performed to identify the promising range, and then a finer search with an interval of 0.01 is carried out between the two best candidates to obtain the optimal setting. Based on this procedure, the best performance is achieved when $K_t = 0.67$ (and $K_T = 0.33$), providing a balanced trade-off between charging time and temperature rise. Table 1 summarizes the parameters used to generate the policy map.

Table 1

Key discretization and weighting parameters for policy map.

Items	Value
SoC interval	every 1 %
Temperature interval	every 2 °C
Current interval	every 0.2 C
Temperature factor (K_T)	0.33
Time factor (K_t)	0.67

For implementation on the microcontroller, the generated policy map is organized as a two-dimensional matrix, where the dimensions are determined by the discretization of temperature and SoC. Bilinear interpolation is subsequently employed to estimate values between the discretized grid points. In the present work, the temperature domain from 15 °C to 45 °C is discretized with a step of 2 °C, while the SoC domain from 10 % to 80 % is discretized with a step of 1 %. Consequently, the policy map for MCU deployment is of dimension 16×71 . Since the temperature and SoC axes are uniformly discretized and do not require additional storage, the size of the policy map is determined by the number of floating-point entries stored in the MCU, as expressed by the following equation:

$$\text{Flash (bytes)} = N_T \times N_{SoC} \times b \quad (14)$$

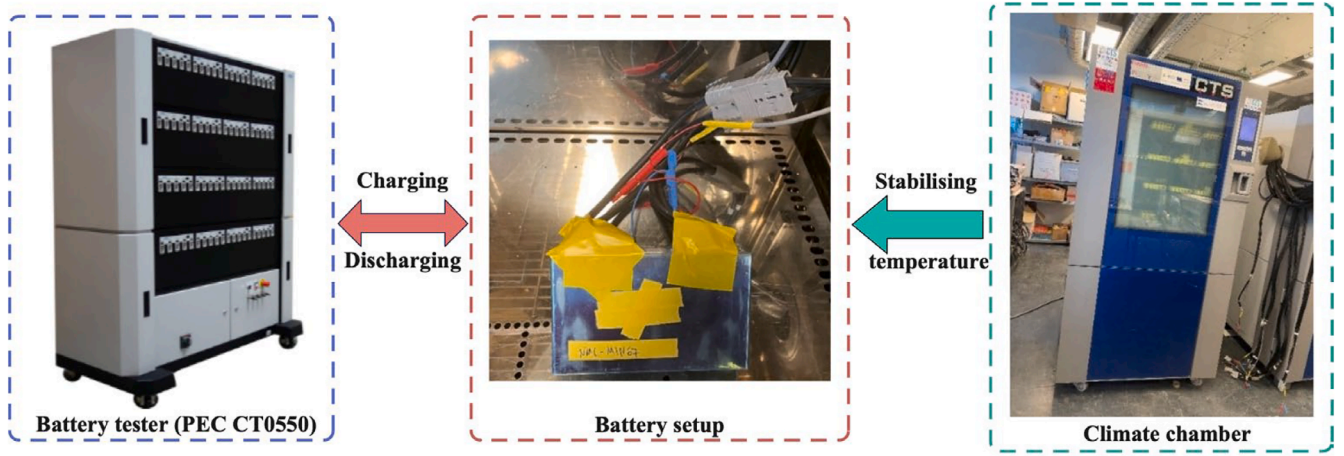
where N_T is the number of discretized temperature points, N_{SoC} is the number of discretized SoC intervals, and b denotes the number of bytes required to store one element in the policy map. For example, using 32-bit floating-point representation requires 4 bytes per entry, resulting in a total memory demand of $16 \times 71 \times 4 = 4544$ bytes (approximately 4.44 KB). Given that the ATmega328P provides 32 KB of Flash, this capacity is sufficient to store the policy map for implementation. In other commonly used microcontrollers, such as the STM32 series with up to 1 MB of Flash, the storage requirement is negligible compared to the available program memory.

4. Experiment setup

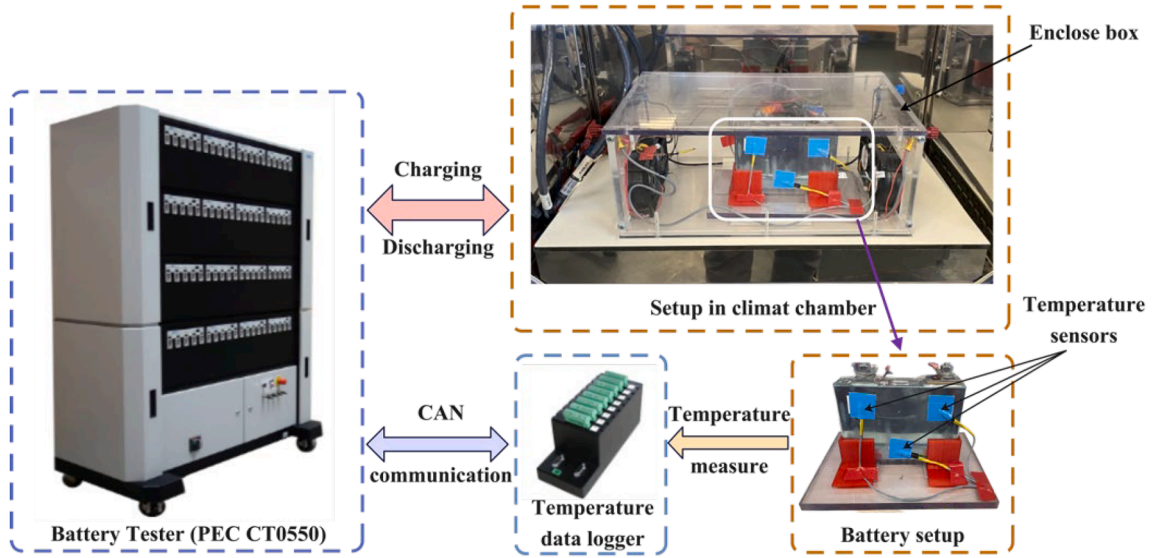
In this study, two different experimental setups are utilized. The first setup focuses on determining battery parameters under different temperatures. As shown in Fig. 5a, the battery is connected to a battery tester (PEC CT0550) and placed inside climate chamber without any cover. Then the OCV and HPPC tests is performed to obtain the battery-electric parameters. In order to obtain the battery-electric parameters as a function of temperature, these two tests are repeated with the climate chamber set to 25 °C, 30 °C and 35 °C respectively.

The second setup focus on validate the electric-thermal model and proposed algorithm. The information about the battery is presented in Table 2, and Fig.5b presents the experiment setup. The battery setup is placed in a CTS climate chamber to ensure a stable and controlled ambient temperature. Simultaneously, to minimize disturbances from the climate chamber fan, the battery setup is enclosed in a box, ensuring that the battery is under natural convection. Note that although there are fans in the box, they are deactivated during the experiment.

Three temperature sensors are positioned on the battery surface to measure its temperature. A temperature data logger with a resolution of ± 0.2 °C is used to capture temperature readings from the sensors and transmit the measured data to the PEC tester via CAN communication. For the charging/discharging of the battery cell, a PEC CT0550 battery tester is utilized, capable of applying a maximum current of 50A for one channel. In this study, the climate chamber is set to 25 °C and 2 channels of the tester are configured together in parallel to perform the experiment achieving a max 100A current. To have a fair comparison with CC charging, the battery is discharged with C/5 current to its minimum voltage, then charged with C/5 current to 10 % SoC, followed by 2 h of resting. After reaching its equilibrium states, the battery is charge with the proposed charging steps and benchmark CC, separately.



(a) Experiment setup for parameter determination



(b) Experiment setup for model and algorithm validation

Fig. 5. Experiment setup for parameter determination and validation.

Table 2
Characteristics of battery.

Characteristic	Value
Nominal voltage	3.65 V
Battery capacity	43 Ah
Battery heat capacity	1015 (J kg ⁻¹ °C ⁻¹) [29]
Battery material	NMC/C
Battery mass	0.94 kg
Battery dimension	L:148 mm x W:27 mm x H:91mm

5. Results and discussion

5.1. Battery parameter

The identified parameters for the battery used in this study are shown in Fig. 6. Within the temperature range of 25 °C to 35 °C, the OCV remains nearly constant agree with literatures [26,27]. The parameter R_0 exhibits temperature dependence, decreasing as the temperature rises, which is reasonable since R_0 represents the internal resistance of the battery and decreases with increasing temperature. Similarly, R_1 is

temperature-dependent and generally decreases with increasing temperature in the mid SoC range (30 % to 70 % SoC). Meanwhile, the capacitance C_1 shows a positive linear relationship with temperature. However, at low SoC ranges, particularly from 10 % to 20 % SoC, this relationship becomes less apparent, possibly due to noise introduced in the HPPC tests, which compromises voltage uniformity when the battery is at a low SoC.

5.2. Model validation

To validate the lumped electro-thermal model, three experiments were conducted using standard constant-current charging rates of 1C, 1.5C, and 2C. Each experiment charged the battery from 10 % to 80 % SoC at a room temperature of 25 °C. Fig. 7(a) shows the simulated and experimental battery temperatures under these charging conditions. The model demonstrates close agreement with the experimental data across all current rates. As shown in Fig. 7(b), the maximum temperature error remains within 1 °C, with RMSE values of 0.111 °C, 0.500 °C, and 0.604 °C for 1C, 1.5C, and 2C, respectively. These results are comparable to recent studies, such as Fan et al. [30], who reported temperature RMSEs of 0.55–0.64 °C under varying ambient conditions and Li et al. [31], who

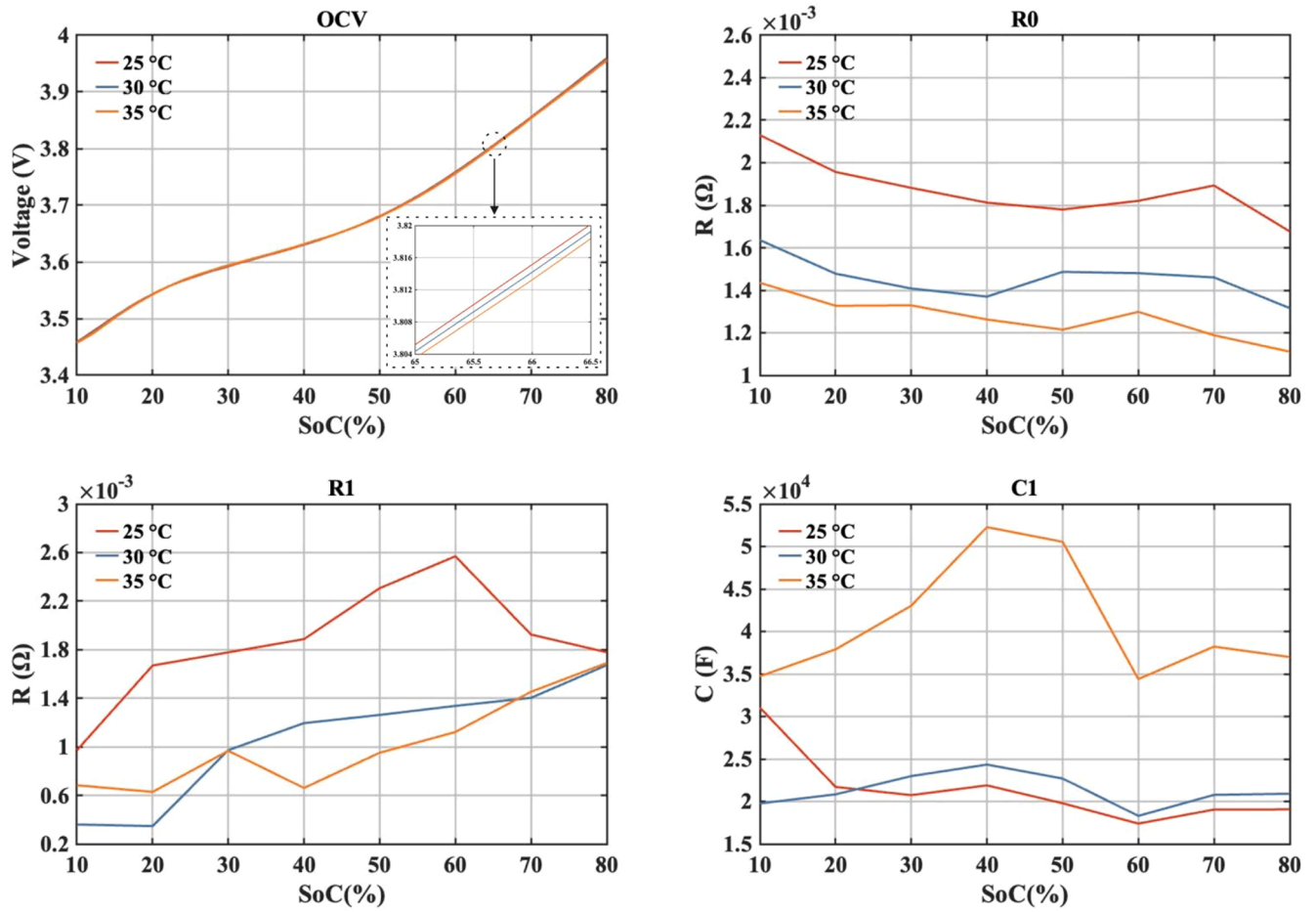


Fig. 6. Determined battery parameters.

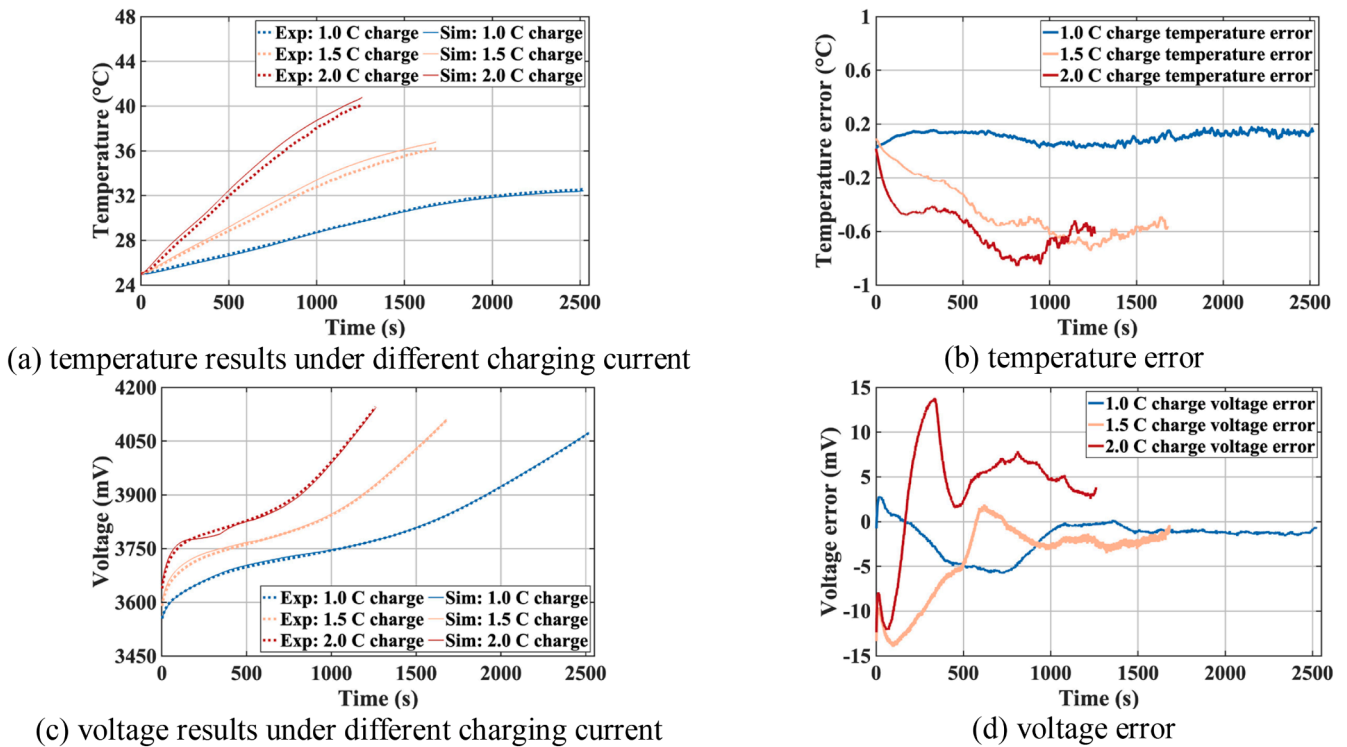


Fig. 7. Experiment and simulation results under different charging currents (charging from 10 % to 80 % SoC).

reported temperature RMSEs of 0.60 °C under fast-charging conditions.

Similarly, the voltage comparison is presented in Fig. 7(c), with detailed error shown in Fig. 7(d). The maximum voltage error is 14 mV in the initial low-SoC region (first 500 s) and remains within 8 mV thereafter. The corresponding RMSE values are 2.659 mV, 5.869 mV, and 7.410 mV for 1C, 1.5C, and 2C charging rates, respectively. These results are consistent with prior work. Kasper et al. [32] demonstrated voltage RMSE reductions of 10.4 mV under dynamic loading, while Xi et al. [33] reported approximately 56.7 mV RMSE for voltage prediction using a neural network-based approach.

5.3. Algorithm validation

The generated optimized policy map controls the current to charge the battery from 10 % to 80 % of the SoC at battery's initial temperature of 25 °C. It is essential to note that while this map is generated under the initial condition of 25 °C and within the 10 % to 80 % SoC range, it dynamically calculates the charging current based on real-time battery status. As a result, it exhibits efficiency across diverse initial SoC levels and temperatures, which will be presented in robustness analysis.

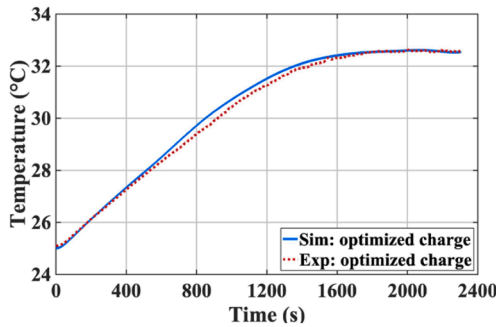
Fig. 8(a) depicts the simulation and experimental results of the battery temperature at the optimized charging current. Initially, the battery temperature rises quickly. Then, from 960 s to 1680 s, the temperature increase slows down. After 1680 s, the temperature stabilizes and stays around 32.5 °C. This behavior aligns with the charging current trend

depicted in Fig. 8(e), wherein the charging current exhibits a high value initially. Then, the current gradually decreases, reaching 39A by the time the charging process approaches completion. And the voltage results of simulation and voltage are shown in Fig. 8(c). Good agreement is found between experimental and simulation results, with a maximum difference of <12 mV shown in Fig. 8(d). The maximum temperature difference between the simulation and the practical temperature during this optimized charging process is <0.4 °C, as shown in Fig. 8(b).

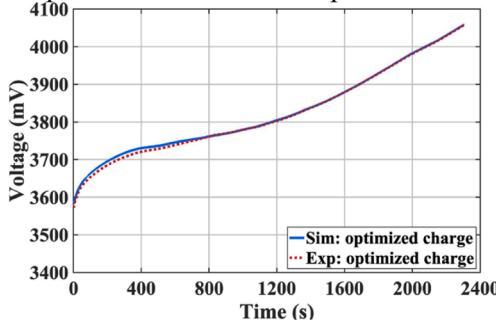
Fig. 8(f) compares the time used for 1C CC charging and optimized charging as they both reach the same temperature at the end of charging. Specifically, 1C CC charging spans 2520 s to charge the battery from 10 % to 80 % of the SoC. In contrast, optimized charging achieves the same level in only 2306 s, resulting in a saving of approximately 8.5 % in charging time. This serves as a demonstration of the algorithm's effectiveness in reducing charging duration without inducing an increase in battery temperature.

5.4. Robustness analysis

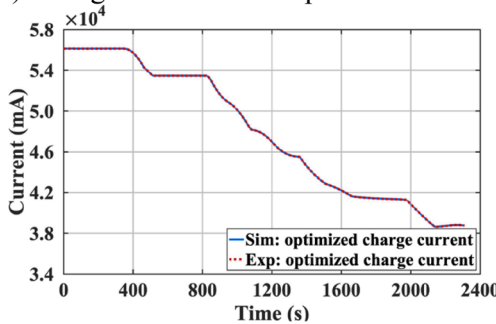
Considering real-life use cases, four different types of scenarios have been studied to assess the robustness of the algorithm. The first scenario assesses the algorithm's resilience by considering a range of different initial and final SoC values. The second scenario assesses the algorithm's robustness under varying initial temperatures, designed to emulate conditions where the battery is charged immediately after operation.



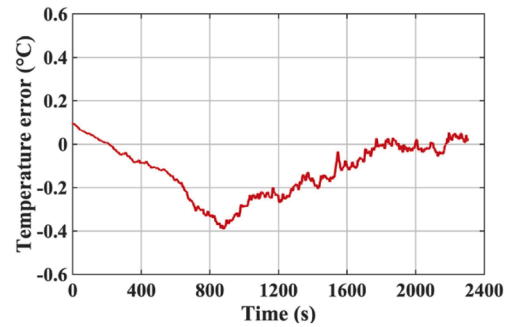
(a) temperature results under optimized charging



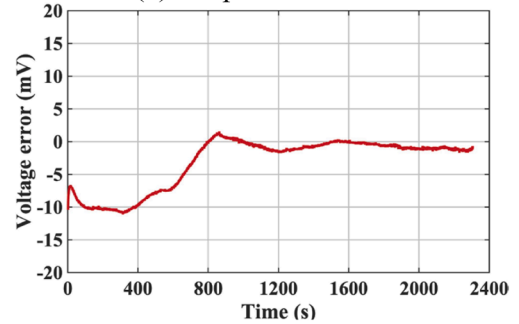
(c) voltage results under optimized charging



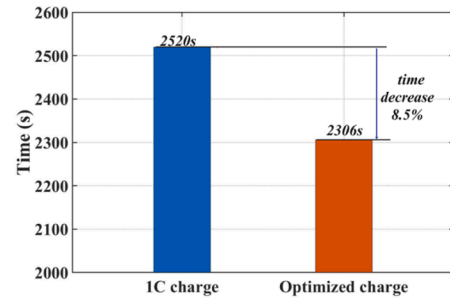
(e) optimized charging current



(b) temperature error



(d) voltage error



(f) time compare between 1C and optimized charging

Fig. 8. Experiment and simulation results for the optimized charging current (charging from 10 % to 80 % SoC).

The third scenario combines the characteristics of the first two cases, representing a typical real-world situation where the user initiates charging shortly after use. In this condition, the battery temperature remains relatively high, and the SoC has not yet decreased to 10 %, closely reflecting common usage patterns. Finally, to assess the robustness of the algorithm across varying SoH, different internal resistance values are incorporated into the simulations to represent the elevated heat generation typically observed in aged batteries.

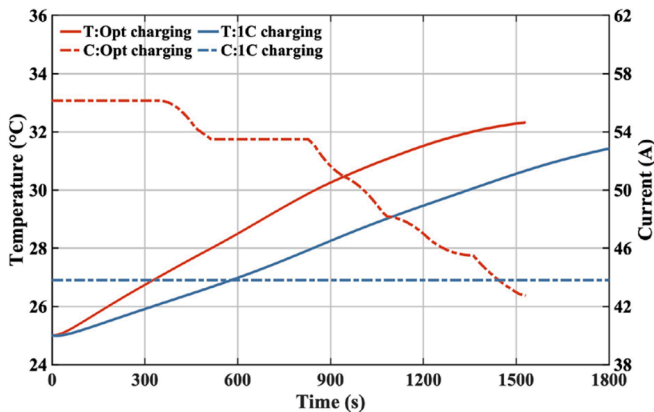
5.4.1. SoC disturbance

Given the variety of charging habits, three cases are considered. The first case initiates charging from 10 % SoC but halts early at 60 % SoC. In the second case, the charging process starts at 30 % SoC and concludes at 80 % SoC. The last case is it starts charging from 20 % SoC and ends at 60 % SoC.

Fig. 9(a) displays the temperature and current profiles during charging from 10 % to 60 % SoC. The behavior of this current and temperature closely resembles the first 1500 s of charging from 10 % to 80 % SoC. This is expected as the policy map returns suggested values based on the current state, and with identical initial conditions, the map returns the same values, resulting in consistent state changes. Fig. 9(b) summarizes the algorithm's performance in this case relative to 1C charging. Despite the maximum temperature rise of approximately 2.8 %, from 31.4 °C to 32.3 °C, the optimized charging method reduces the charging time from 1800 s to 1530 s, achieving a time savings of about 15 % compared to 1C charging.

Fig. 10(a) illustrate the current and temperature profiles during charging from 30 % to 80 % SoC. In this case, the behavior of current and temperature deviates from that observed during charging from 10 % to 80 % SoC. This difference is attributed to the varying initial state, as previously discussed, which influences the charging dynamics throughout the period. When compared with 1C charging is depicted in Fig. 10(b), the temperature difference at the end of charging in this case is <1 % compared to 1C charging. Nonetheless, significant time savings are achieved: approximately 7.3 % (from 1800s to 1668s).

Fig. 11(a) illustrate the current and temperature profiles during charging from 20 % to 60 % SoC. The algorithm adapted the charging current behavior compared to the scenario charging from 10 % to 80 %. Notably, the charging process terminates before reaching the algorithm's expected stabilization temperature, prompting the algorithm to continue raising the battery temperature throughout the charging. Consequently, the temperature difference compared with 1C charging is relatively higher around 2.6 %, as illustrated in Fig. 11(b). However, the time savings are significant, amounting to approximately 14.4 %.



(a) Optimized charging temperature and current

5.4.2. Initial temperature disturbance

To assess the robustness of the algorithm about the battery initial temperature, two distinct initial temperatures are selected. One set the initial temperature to 27 °C to simulate battery charging immediately after normal use, while the other set the initial temperature to 30 °C to simulate charging immediately after heavy use.

Fig. 12(a) presents the temperature and current profiles during charging with an initial temperature of 27 °C. Compared to the 25 °C case, the algorithm adjusts the current more gently, reaching 56A only for the first 350 s and then gradually decreasing. After 722 s, the current drops further to 38 A by the end of charging. This adjustment helps maintain thermal stability once the target temperature is approached earlier due to the higher initial temperature. As shown in Fig. 12(b), the maximum temperature remains comparable to that under 1C charging, while the charging time is reduced by approximately 7.7 %.

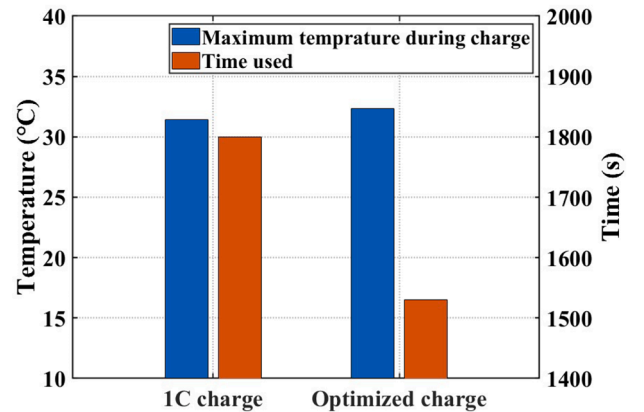
As shown in Fig. 13(a), when the initial temperature is 30 °C, the 1C charging temperature first drops in the initial 500 s due to the 5 °C difference from ambient, then rises as heat generation overtakes heat dissipation. In contrast, the proposed algorithm leverages this early thermal advantage by applying higher current initially, then gradually reducing it to maintain temperature stability. As illustrated in Fig. 13(b), the peak temperature is similar to 1C charging, but the total charging time is reduced by approximately 6.0 %, demonstrating the robustness of this algorithm.

5.4.3. Mixing with SoC and initial temperature disturbances

In this scenario, to simulate a realistic situation where the user begins charging the battery immediately while the SoC has not yet reached 10 %, a charging range from 20 % to 70 % SoC at an initial temperature of 27 °C is used. The results of temperature and current are shown in Fig. 14(a). As in other cases, the algorithm initially increases the temperature and then maintains it at a stable level, according to the predetermined expectations of the algorithm. Fig. 14(b) presents the comparison between 1C and optimized charging. Similar to other cases, the strategic approach used by the algorithm maintains the maximum temperature difference to <1.5 % compared with 1C charging. Furthermore, the charging time is reduced by approximately 9.4 %, demonstrating the robustness of this algorithm in the mixed scenario.

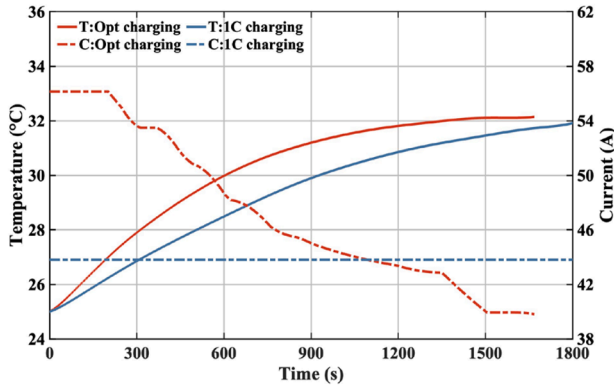
5.4.4. Increased internal resistance

To evaluate the performance of the proposed algorithm with aged batteries, the effect of increased internal resistance was simulated. Since the internal resistance of lithium-ion batteries tends to rise with aging [34,35], leading to elevated heat generation, simulations were performed with resistance values scaled to $1.5 \times$ and $2 \times$ the nominal value R_0 . In practice, cells with internal resistance above $2 \times$ the nominal

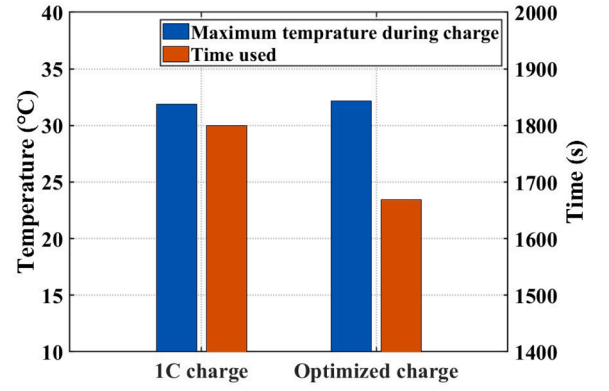


(b) Results comparison with 1C charging

Fig. 9. Robustness analysis of SoC disturbance (charging from 10 % to 60 % SoC).

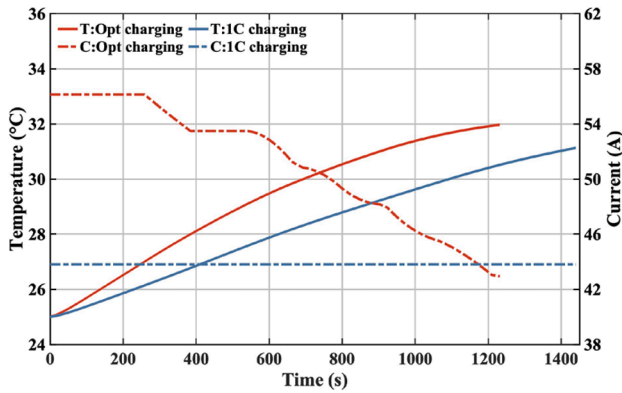


(a) Optimized charging temperature and current

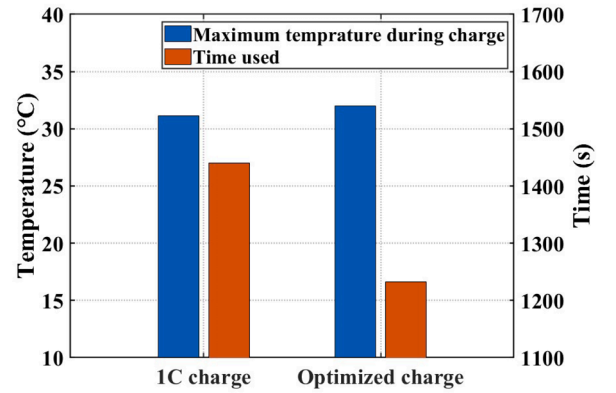


(b) Results comparison with 1C charging

Fig. 10. Robustness analysis of SoC disturbance (charging from 30 % to 80 % SoC).

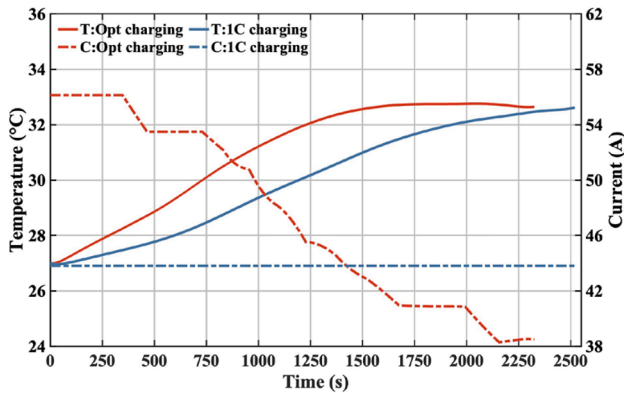


(a) Optimized charging temperature and current

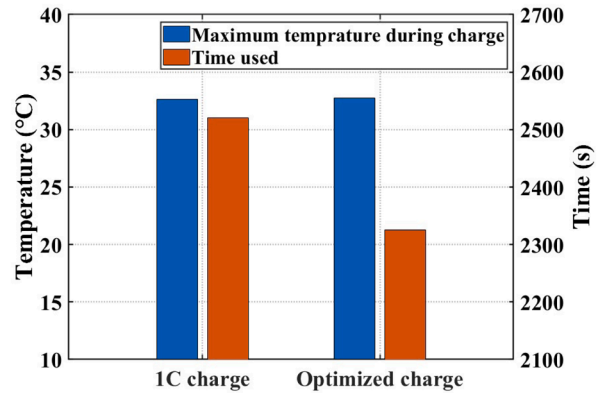


(b) Results comparison with 1C charging

Fig. 11. Robustness analysis of SoC disturbance (charging from 20 % to 60 % SoC).



(a) Optimized charging temperature and current



(b) Results comparison with 1C charging

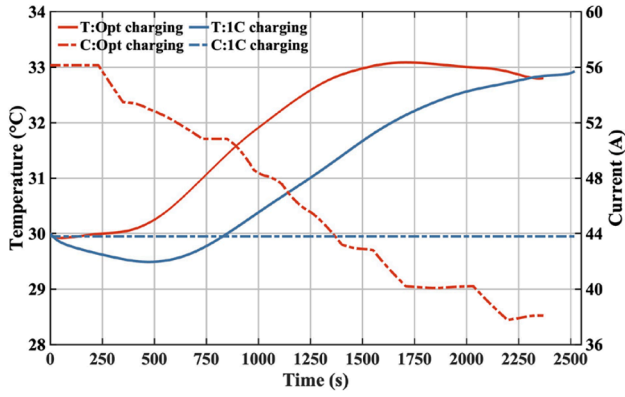
Fig. 12. Robustness analysis of initial temperature disturbance (initial temperature at 27 °C).

value are unsuitable for high-rate operations. Hence, the analysis was limited to $2 \times R_0$. The results, summarized in Fig. 15, show that under $1.5 \times R_0$, the proposed algorithm completed charging in 2389 s with a maximum temperature of 33.58 °C. In contrast, conventional 1C charging required 2520 s and reached a slightly higher temperature of 33.88 °C, yielding a 5.1 % reduction in charging time. Under $2 \times R_0$, the algorithm maintained the maximum temperature below 35 °C while reducing the charging duration by 2 % compared to 1C charging, which exceeded 35 °C. These results demonstrate that the proposed algorithm

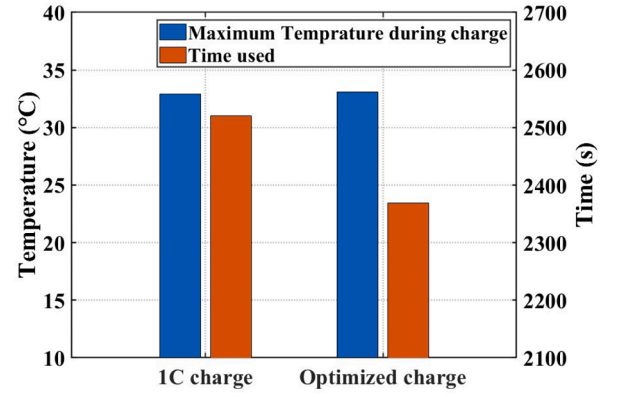
remains effective and thermally safe under aged-battery conditions.

5.5. Real-time runtime analysis

To verify the feasibility of the proposed algorithm on low-cost microprocessor, two distinct microprocessor have been chosen for performance assessment, as detailed in Table 3. The optimized policy map is integrated into the microprocessor. The algorithm execution time is recorded from the input of battery status to the retrieval of the

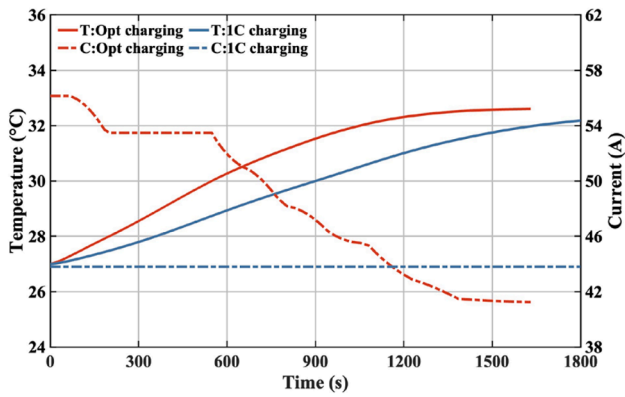


(a) Optimized charging temperature and current

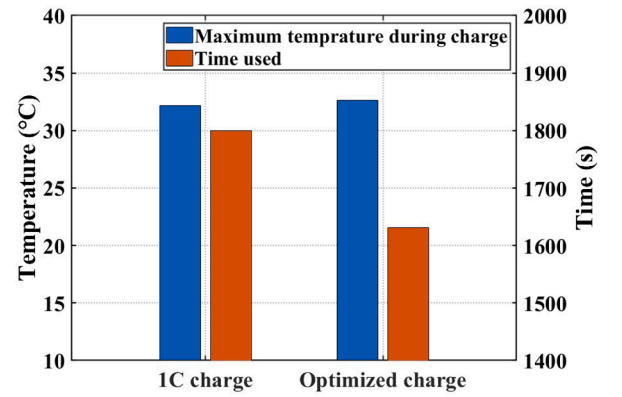


(b) Results comparison with 1C charging

Fig. 13. Robustness analysis of initial temperature disturbance (initial temperature at 30 °C).



(a) Optimized charging temperature and current



(b) Results comparison with 1C charging

Fig. 14. Robustness analysis of mixing with SoC and initial temperature disturbance.

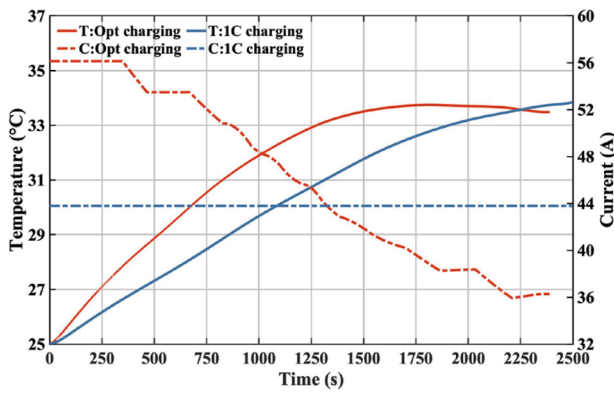
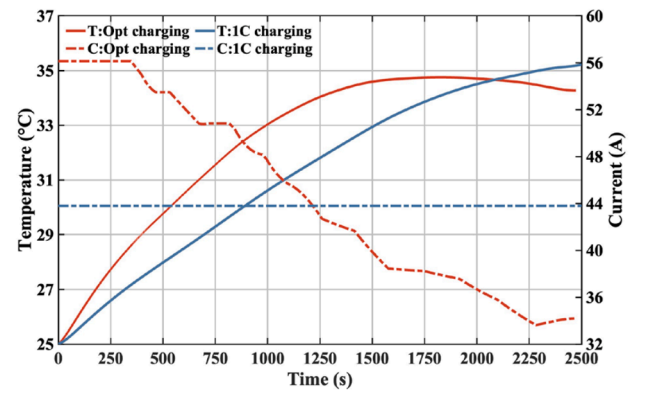
(a) Charging profile at $R=1.5 \times R_0$ (b) Charging profile at $R=2.0 \times R_0$

Fig. 15. Robustness analysis of Increased internal resistance.

Table 3

Execution on different processors.

	ATmega328	Atmel SAM3 × 8E
Processor architecture	8-bit AVR®	32-bit ARM® Cortex®-M3
Frequency	16 MHz	84 MHz
Execution time	0.44 ms	0.073 ms

recommended current from the policy map. All interrupts were disabled and no background tasks were running during the test, in order to measure the algorithm's execution time under controlled condition. The results demonstrate that the proposed algorithm can successfully run on a low-cost microprocessor. It takes 0.44 milliseconds to run once on an 8-bit microprocessor with a frequency of 16 MHz, and 0.076 milliseconds to run once on a 32-bit microprocessor with a frequency of 84 MHz.

5.6. Limitations

The proposed charging strategy demonstrates promising performance under room-temperature conditions and is well-suited for low-cost microcontroller deployment. However, two main limitations should be noted. First, extreme temperature conditions (e.g., sub-zero temperatures or above 40 °C) were not included in the experimental validation due to restrictions in the battery's operational specifications. Second, the current model does not account for battery aging effects, such as the increase in internal resistance over charge–discharge cycles. These factors may affect long-term performance in real-world applications. Future work will address these issues by incorporating aging-aware parameter adaptation and integrating charging control with thermal conditioning strategies, such as preheating at low temperatures and cooling at high temperatures.

6. Conclusion

In this study, a fast-charging optimization algorithm is proposed for electric micromobility devices equipped with lithium-ion batteries. Considering the limited computing power of these devices, the proposed algorithm requires only low computational effort when running in real time. To do so, the algorithm incorporates both offline training and online operation. In offline training, a comprehensive electro-thermal model is presented, encompassing both reversible and irreversible heat generation within the battery. The charging process is then divided into several stages by different start and end SoC. The model is then used to calculate a state grid based on different initial temperatures, which includes the charging temperature and charging time for each stage of charging. Dynamic programming is then used to find the optimal charging current based on the cost of the state grid to form an optimized policy map based on the battery status. In real-time operation, the processor simply interpolates the optimized policy map based on the battery's current state to obtain the optimized charging current. The experimental and simulation results indicate that the proposed algorithm reduces charging time while maintaining a similar temperature rise. The robustness analysis shows that the algorithm performs well at different initial room temperatures and SoC ranges. When executed once, the algorithm achieves a minimum execution time of 0.44 ms on an 8-bit microprocessor and 0.073 ms on a 32-bit microprocessor. These results demonstrate the efficiency and stability of the proposed algorithm.

While the proposed strategy has demonstrated promising performance under room-temperature conditions, certain aspects remain beyond the current scope. Specifically, extreme temperature conditions (e.g., sub-zero or above 40 °C) were not included in the experimental validation, as the tested battery cells are not specified for operation in such environments. In addition, the present model does not explicitly account for battery aging effects, such as gradual increases in internal resistance over time, which could influence long-term performance. Future research will aim to address these aspects by incorporating aging-aware parameter adaptation and integrating charging control with thermal conditioning strategies, including preheating at low temperatures and cooling at elevated temperatures. Extension of the proposed method to battery modules and multi-cell pack-level systems will also be investigated to evaluate its scalability in more complex configurations.

CRedit authorship contribution statement

Jiacheng He: Writing – review & editing, Writing – original draft, Methodology, Investigation. **Theodoros Kalogiannis:** Supervision. **Xia Zeng:** Writing – review & editing, Resources. **Md Sazzad Hosen:** Writing – review & editing, Data curation. **Maitane Bercibar:** Writing – review & editing, Supervision.

Declaration of competing interest

The authors declare the following financial interests/personal relationships which may be considered as potential competing interests: Jiacheng He reports a relationship with VUB University that includes: employment and funding grants. If there are other authors, they declare that they have no known competing financial interests or personal relationships that could have appeared to influence the work reported in this paper.

Acknowledgement

The authors would like to acknowledge the support of the Electromobility Research Centre (MOBI) at Vrije Universiteit Brussel (VUB) and the NEMO project funded by the European Union's Horizon Europe research and innovation program under Grant Agreement No 101102944.

Data availability

The authors do not have permission to share data.

References

- [1] G. Ramkumar, S. Kannan, V. Mohanavel, S. Karthikeyan, A. Titus, The future of green mobility: a review exploring renewable energy systems integration in electric vehicles, *Results Eng.* 27 (2025).
- [2] Z. An, L. Jia, Y. Ding, C. Dang, X. Li, A review on lithium-ion power battery thermal management technologies and thermal safety, *J. Therm. Sci.* 26 (2017) 391–412.
- [3] J. Lin, X. Liu, S. Li, C. Zhang, S. Yang, A review on recent progress, challenges and perspective of battery thermal management system, *Int. J. Heat. Mass Transf.* (2021) 167.
- [4] M.M. Hamed, A. El-Tayeb, I. Moukhtar, A.Z. El Dein, E.H. Abdelhameed, A review on recent key technologies of lithium-ion battery thermal management: external cooling systems, *Results Eng.* 16 (2022).
- [5] F.S. Hwang, T. Confrey, C. Reidy, D. Picovici, D. Callaghan, D. Culliton, C. Nolan, Review of battery thermal management systems in electric vehicles, *Renew. Sustain. Energy Rev.* (2024) 192.
- [6] D. Karimi, H. Behi, J. Van Mierlo, M. Bercibar, Experimental and numerical analysis of holistic active and passive thermal management systems for electric vehicles: fast charge and discharge applications, *Results Eng.* 15 (2022).
- [7] N. Wassiliadis, J. Schneider, A. Frank, L. Wildfeuer, X. Lin, A. Jossen, M. Lienkamp, Review of fast charging strategies for lithium-ion battery systems and their applicability for battery electric vehicles, *J. Energy Storage* (2021) 44.
- [8] C. Chen, Z. Wei, A.C. Knoll, Charging optimization for Li-ion battery in electric vehicles: a review, *IEEE Trans. Transp. Electr.* 8 (2022) 3068–3089.
- [9] S. Duan, K. Xia, J. Li, Z. Zhao, H. Liu, Optimization charging method of lithium-ion battery based on multi-objective BBO algorithm, *J. Energy Storage* (2024) 91.
- [10] K. Shen, J. Dai, Y. Zheng, C. Xu, R. Zhang, H. Wang, C. Jin, X. Han, X. Lai, X. Qian, X. Feng, Closed-loop fast charging strategy of lithium-ion batteries based on temperature limitation and lithium precipitation, *Therm. Sci. Eng. Prog.* (2023) 46.
- [11] K. Sayed, M. Aref, M.M. Almalki, M.A. Mossa, Optimizing fast charging protocols for lithium-ion batteries using reinforcement learning: balancing speed, efficiency, and longevity, *Results Eng.* (2025) 25.
- [12] H.E. Ouazzani, I.E. Hassani, N. Barka, T. Masrour, MSCC-DRL: multi-stage constant current based on deep reinforcement learning for fast charging of lithium ion battery, *J. Energy Storage* (2024) 75.
- [13] L. Chen, Y. Tao, A.M. Lopes, M.-Y. Chow, Y. Chen, Safety-optimized fast charging of lithium-ion battery based on distributional SAC-conservative augmented lagrangian SDR algorithm, *IEEE Trans. Veh. Technol.* 74 (2025) 12016–12028.
- [14] S.S. Saha, S.S. Sandha, M. Srivastava, Machine Learning for microcontroller-class hardware: a review, *IEEE Sens. J.* 22 (2022) 21362–21390.
- [15] Z. Wang, C. Hu, Z. Zheng, Z. Feng, X. Si, H. Wang, Theoretical analysis and case application of intelligent joint predictive ordering-replacement policy driven by real-time prognostics for IMU, *IEEE Trans. Consum. Electron.* (2025), 1–1.
- [16] W. Liu, T. Placke, K.T. Chau, Overview of batteries and battery management for electric vehicles, *Energy Rep.* 8 (2022) 4058–4084.
- [17] C.-H. Lee, T.-W. Chang, S.-H. Hsu, J.-A. Jiang, Taguchi-based PSO for searching an optimal four-stage charge pattern of Li-ion batteries, *J. Energy Storage* 21 (2019) 301–309.
- [18] L. Jiang, Y. Li, Y. Huang, J. Yu, X. Qiao, Y. Wang, C. Huang, Y. Cao, Optimization of multi-stage constant current charging pattern based on Taguchi method for Li-ion battery, *Appl. Energy* (2020) 259.
- [19] X. Wu, Y. Xia, J. Du, X. Gao, S. Nikolay, Multistage constant current charging strategy based on multiobjective current optimization, *IEEE Trans. Transp. Electr.* 9 (2023) 4990–5001.
- [20] K. Kumar, K. Pareek, Fast charging of lithium-ion battery using multistage charging and optimization with Grey relational analysis, *J. Energy Storage* (2023) 68.

- [21] Q.-Y. Huang, Y.-H. Liu, G.-J. Chen, Y.-F. Luo, C.-L. Liu, Optimization of the SOC-based multi-stage constant current charging strategy using coyote optimization algorithm, *J. Energy Storage* (2024) 77.
- [22] M.U. Tahir, A. Sangwongwanich, D.-I. Stroe, F. Blaabjerg, Multi-objective optimization for multi-stage constant current charging for Li-ion batteries, *J. Energy Storage* 86 (2024).
- [23] T.M. Bandhauer, S. Garimella, T.F. Fuller, Temperature-dependent electrochemical heat generation in a commercial lithium-ion battery, *J. Power Sources* 247 (2014) 618–628.
- [24] A.F. Gunnarshaug, P.J.S. Vie, S. Kjelstrup, Review—Reversible heat effects in cells relevant for lithium-ion batteries, *J. Electrochem. Soc.* (2021) 168.
- [25] M. Akbarzadeh, T. Kalogiannis, J. Jaguemont, J. He, L. Jin, M. Bercebar, J. Van Mierlo, Thermal modeling of a high-energy prismatic lithium-ion battery cell and module based on a new thermal characterization methodology, *J. Energy Storage* (2020) 32.
- [26] J. He, M. Sazzad Hosen, R. Youssef, T. Kalogiannis, J. Van Mierlo, M. Bercebar, A lumped electro-thermal model for a battery module with a novel hybrid cooling system, *Appl. Therm. Eng.* (2023) 221.
- [27] X. Lin, H.E. Perez, S. Mohan, J.B. Siegel, A.G. Stefanopoulou, Y. Ding, M. P. Castanier, A lumped-parameter electro-thermal model for cylindrical batteries, *J. Power Sources* 257 (2014) 1–11.
- [28] T. Kalogiannis, M.S. Hosen, F.H. Gandoman, M.A. Sokkeh, J. Jaguemont, M. Bercebar, J. Van Mierlo, Multi-objective particle swarm optimization and training of datasheet-based load dependent lithium-ion voltage models, *Int. J. Electr. Power Energy Syst.* (2021) 133.
- [29] J. He, R. Youssef, M.S. Hosen, M. Akbarzadeh, J. Van Mierlo, M. Bercebar, A novel methodology to determine the specific heat capacity of lithium-ion batteries, *J. Power Sources* 520 (2022).
- [30] X. Fan, W. Zhang, H. Qi, X. Zhou, Accurate battery temperature prediction using self-training neural networks within embedded system, *Energy* (2024) 313.
- [31] S. Li, C. Zhang, Y. Zhao, G.J. Offer, M. Marinescu, Effect of thermal gradients on inhomogeneous degradation in lithium-ion batteries, *Commun. Eng.* 2 (2023).
- [32] J. Kasper, P. Hrzina, L. Cerná, T. Finsterle, V. Knap, Kinetic model for improved dynamic current response in lithium-ion battery electrical circuit models, *Monatsh. Chem. - Chem. Mon.* 156 (2025) 539–548.
- [33] H. Xi, T. Lv, J. Qin, M. Ma, J. Xie, S. Lu, Z. Liu, Prediction of lithium battery voltage and State of charge using multi-head attention BiLSTM neural network, *Appl. Sci.* (2025) 15.
- [34] P. Li, Z. Ao, J. Hou, S. Xiang, Z. Wang, Physics-informed mamba neural network with potential knowledge for state-of-charge estimation of lithium-ion batteries, *J. Energy Storage* (2025) 123.
- [35] P. Li, X. Wu, R. Grosu, J. Hou, M. Ilolov, S. Xiang, Applying neural network to health estimation and lifetime prediction of lithium-ion batteries, *IEEE Trans. Transp. Electr.* 11 (2025) 4224–4248.